Nanoporous gold by dealloying of an amorphous precursor

Nanoporous gold by dealloying of an amorphous precursor

P.Rizzi, F.Scaglione, L.Battezzati

Dipartimento di Chimica and NIS, Università di Torino, V. Giuria 7, 10125 Torino, Italy.

Abstract

Nanoporous gold has been produced by the electrochemical dealloying of a $Au_{40}Cu_{28}Ag_7Pd_5Si_{20}$ metallic glass. Suitable conditions of potential and temperature of dealloying have been established from polarization curves and dealloying has been conducted at the critical potential of 1.05 V in three different electrolytes: 1 M HNO_3, 1 M $HClO_4$ and 1 M H_2SO_4. The resulting material after 6 hour of dealloying was constituted by ligaments made of pure Au and pores. The morphology was determined by SEM: ligaments of about 100 nm was observed and their size appears slightly larger (130 nm) when HNO_3 is used.

In the first stages of dealloying (30 - 300 s), nanopores and nanocrystals, randomly oriented, were found by HRTEM. From these observations a diffusivity value for crystal growth was estimated. A change in growth mechanism was suggested when impingement occurs for long dealloying times.

It is suggested that the ligament and pore morphology can be tailored in order to obtain materials with different chemical and physical properties.

Keywords: A. metallic glasses; C. diffusion; C. corrosion; C. electrochemical reactions; D. scanning electron microscopy, SEM; D. X-ray diffraction

1. Introduction

Nanoporous metals have achieved an important place in literature, because of different possible applications such as catalysis [1, 2], surface-enhanced Raman scattering [3, 4] and actuators [5]. They can be prepared by electrochemical dealloying of a metallic precursor that can be either crystalline or amorphous. During dealloying, the less noble elements of the alloy are removed while

the atoms of the noble element reorganise themselves by surface diffusion [6, 7] forming ligaments and porosities that can have dimensions of the order of tens of nanometers. When the precursor is a crystalline alloy, the ligaments retain the crystallographic orientation of the grain from which they originate and have angular displacement of a few degrees between each other [8]. On the contrary, when dealloying of amorphous alloys is undertaken, the non crystalline structure and the absence of grain boundaries suggest that nucleation and growth of crystals must occur to form ligaments. The process parameters that play a role during dealloying are: the difference in electrochemical potential between the alloy components, the critical potential for corrosion [9, 10], the amount of noble element i.e. the parting limit [11, 12], the composition, pH and temperature of the electrolyte. The influence of the process parameters on the final morphology of ligaments and pores is not yet completely understood and it is of interest to study this correlation for applications requiring the design of specific patterns. In particular the effect of the electrolyte on the dimension of ligaments and pores is not jet completely understood for dealloying of crystalline precursors and it has not been analysed for dealloying of amorphous alloys. Moreover, little is known in literature on the mechanism of dealloying when an amorphous alloy is used as a precursor.

In this paper, we report on the production of nanoporous gold starting from a $Au_{40}Cu_{28}Ag_7Pd_5Si_{20}$ amorphous alloy by means of electrochemical etching. Different electrolytes are used in order to compare the morphologies obtained. Moreover, the first stages of the dealloying are examined and a mechanism of dealloying is proposed based on of High Resolution Transmission Electron Microscopy observations.

2. Experimental

Ingots of composition $Au_{40}Cu_{28}Ag_7Pd_5Si_{20}$ were prepared by arc-melting the pure elements (Au: 99.99%, Ag, Cu and Pd: 99.99%, Si: 99,9995%) in Ar atmosphere and using Ti getters. Ribbons about 25 μm thick and 2 mm wide were obtained completely amorphous by melt spinning using a linear velocity of the copper wheel of 22 m/s. Samples of 15 mm in length were cut from ribbons.

Detailed information on production and characterization of the as spun ribbon are reported in a previous work [13].

A Potentiostat/Galvanostat (Model 7050, Amel Instruments) has been used for electrochemical de-alloying. The cell is composed of the sample as working electrode, a Pt counter electrode and a Ag/AgCl reference electrode; a double bridge configuration has been employed to avoid deposition of the de-alloyed ions as insoluble salts.

The critical potential for dealloying has been determined by performing polarization curves as a function of the temperature of the electrolyte [10]. Once the suitable conditions for etching have been found, i.e. 1.05 V (vs Ag/AgCl) at 70 °C, electrochemical dealloying has been performed in three different electrolytes: 1 M HNO_3, 1 M $HClO_4$ and 1 M H_2SO_4 for 6 hours.

Ribbons have been analyzed before and after electrochemical etching using X-ray diffraction (XRD) in Bragg-Brentano geometry with monochromatic Cu Kα radiation, Scanning Electron Microscopy (SEM), Energy Dispersive X-ray Spectroscopy (EDS) (calibrated with a pure Co sample). Transmission Electron Microscopy (TEM) observations were done with samples thinned by mechanical polishing and, successively, electrochemically etched for 30 s and 300 s with the procedure specified above.

3. Results and Discussion

3.1. Electrochemical behaviour

In order to determine the critical potential for de-alloying, the electrochemical behavior was studied by performing polarization curves with a scan rate of 5 mV/s, using as electrolyte 1 M H_2SO_4 solution at different temperatures. Results are shown in Fig 1. At room temperature the sample shows an excellent corrosion resistance due to the presence of a passivation zone extended from 0.53 V to about 1 V (vs Ag/AgCl) and characterized by low current densities of the order of 10^{-6}-10^{-5} A/cm^2. In the anodic branch of the curve an active region appears at about 1 V where the current density reaches higher values. The passivation zone is followed at higher potential values by the

trans-passivation zone, where the current density increases rapidly.

When polarization curves are performed at higher temperatures, a similar trend is observed as the one described for the RT experiment, but the current densities raise in the whole range of potential as the temperature is increased. The E_{corr} values generally decrease with increasing temperature although with some scatter probably due to the state of the surface of individual samples. This has, however, no influence on the current densities at higher potential.

Polarization curves in 1 M HNO_3 and 1 M $HClO_4$ at 70 °C show that the active region for dealloying is maintained and the current density at 70 °C follows the trend $HNO_3 > H_2SO_4 > HClO_4$ over the whole range of potentials.

The critical potential E_c has been fixed for all electrolytes as 1.05 V, where the current densities are. The temperature of 70 °C was chosen in order to have current densities of the order of 1 $mAcm^{-2}$ (4.3×10^{-3} Acm^{-2}, 4.2×10^{-4} Acm^{-2}, 1.7×10^{-4} Acm^{-2} for HNO_3, H_2SO_4 and $HClO_4$ respectively) which allows extensive etching of ribbon samples in times of a few hours as previously demonstrated [13]. Moreover, at 70°C and 1.05 V (vs Ag/AgCl) no fracture of samples due to stress corrosion cracking [14, 15, 16] was observed. On the contrary, for $Au_{40}Cu_{28}Ag_7Pd_5Si_{20}$ samples dealloyed in the transpassive zone at various temperatures and at potentials in excess of 1.6 V, where high current densities are acting, an extended phenomenon of stress corrosion cracking was always observed.

3.2. Dealloying morphologies and mechanism of dealloying

Diffraction patterns of samples dealloyed in different solutions (Fig. 2) show that the amorphous halo disappears and reflections of an fcc phase based on Au occur. Rietveld analysis [17] of diffraction patterns indicate that the lattice constant (a_0) for all samples is always compatible with pure Au within the experimental error and that the size of the crystalline domains is 48 ± 4 nm, 49 ± 4 nm and 61 ± 6 nm for the samples dealloyed in 1 M $HClO_4$, 1 M H_2SO_4 and 1 M HNO_3 respectively.

Secondary electrons SEM images of dealloyed samples are reported in Fig. 3. As can be seen from

cross section images, all samples were completely dealloyed. The size of pores and ligaments appears homogeneous on both surfaces (air and wheel-side) and within the cross section of each sample showing that the dealloying mechanism remains the same on the surface and in the inner part of the sample. Ligaments and pores appear finer in the sample dealloyed by perchloric and sulfuric acid than those obtained in nitric acid. The average ligament sizes are 98 ± 24 nm, 91 ± 22 nm and 131 ± 34 nm for 1 M $HClO_4$, 1 M H_2SO_4 and 1 M HNO_3 respectively. EDS analysis shows that ligaments are made of Au in all samples and that the other elements are below the detection limit of the instrument, confirming the inference from lattice constants. The produced nanoporous ribbon is a free standing material that can be bent without cracking.

In order to determine the morphology and microstructure in the initial stages of the process a $Au_{40}Cu_{28}Ag_7Pd_5Si_{20}$ sample was dealloyed for 30 s in 1 M HNO_3 and then observed by TEM. From High Resolution images (HRTEM) it is apparent that rounded nanocrystals of average size of 5 nm are formed, oriented in different directions (Fig. 4, HRTEM) and small nanopores appears on the surface of the sample. From HRTEM lattice fringes, the interplanar spacing of the (111) plane was determined to be 2.24 ± 0.03 Å, value slightly lower then pure Au. Therefore, the presence of other elements in solid solution with Au at this stage can be envisaged. When dealloying is performed for 300 s, a similar morphology appears with crystals roughly doubled in size, showing that crystal growth occurs immediately when Au atoms, freed of their local environment, move by surface diffusion from the inner layers of the ribbon. At this stage, the interplanar spacing of the (111) plane determined from HRTEM was 2.26 ± 0.04 Å, confirming the formation of an Au based solid solution. When the dealloying process is performed for longer times, progressive leaching with consequent nucleation of crystals in the inner part of the sample occurs as soon as pores become available to allow penetration of the electrolyte to reach the underlying amorphous alloy. It can be expected that, at this stage, an impingement of crystals growing in different directions occurs that limits further increase in crystal size by diffusion and that change the mechanism of ligament growth. Therefore, ligaments formed by multiple crystals can be expected when an amorphous

precursor is extensively dealloyed, contrary to what observed in crystalline alloys where the original grain orientation is retained in the final nanoporous material. This mechanism explains the difference in size of the crystalline domains determined from the XRD patterns and of the ligaments determined by SEM.

3.3. Surface gold diffusion

Being dealloying a process controlled by a surface diffusion mechanism, the values of surface diffusivity of gold adatoms can be evaluated by the following equation [18, 19, 20] which was proposed in connection to the change in roughness of the surface of noble elements electrodes:

$$D_s = \frac{d(t)^4 kT}{32\gamma t a_0^{\ 4}} \qquad (1)$$

where k is the Boltzmann constant, T the dealloying temperature (K), γ the surface energy (1 Jm^{-2} [21]), t the dealloying time (s), a_0 the lattice parameter of gold (4.08×10^{-10} m); d(t) is the radius of the coalescing particles. In the literature, when dealloying of crystalline alloys was considered, the d(t) was associated with the ligament diameter. In the amorphous precursors case, on the contrary, for d(t) the size of the crystals has to be taken into account instead of that of ligaments. Moreover, since a change in mechanism for growth is envisaged due to impingement after the first stages of dealloying, the diffusivity can be correctly determined only from data collected in the initial stages of the process. Therefore, in the case of the sample dealloyed in 1 M HNO_3, D_s was evaluated taking into account the crystal size determined by HRTEM in the samples dealloyed for 30 s and 300 s, obtaining 1×10^{-19} m^2s^{-1}. This value is much higher than the diffusion of surface gold atoms in contact with vacuum (1×10^{-30} m^2s^{-1} [22]). This could be expected due to the presence of the electrolyte solution; in fact, a partial loss of the metallic character of the Au atoms was claimed due to an interaction of the partial empty gold orbitals with the sp^3 orbital of the water molecules that will produce a relaxation of the surface [22]. Moreover, when Au atoms remain on the surface without lateral coordination due to the leaching of the less noble elements, they tend to diffuse in

order to constitute agglomerates so that the total surface energy is decreased. In the literature, a few diffusivity values are reported for dealloying, mostly in free corrosion conditions or for less concentrated electrolytes in electrochemical dealloying conditions: diffusivity values vary in a range from 2×10^{-20} m^2s^{-1} ($HClO_4$ 0.1M at 25°C [21]) to 5×10^{-18} m^2s^{-1} (H_2SO_4 0.5 M at 25°C [23]). In this work, using the described processing conditions, similar diffusivity is obtained, showing the reason for rapid growth of gold nanocrystals in the first stage of the dealloying process.

3.4 Effect of the electrolyte on the final morphology

The effect of the electrolyte used for dealloying can be explained taking into account the considerations made in the previous paragraphs on the mechanism of dealloying and on the diffusivity. It was observed by SEM that the morphology after complete dealloying (ligament and pore sizes) is slightly coarsened when HNO_3 is used with respect to $HClO_4$ and H_2SO_4. This could be due to the rate of leaching of the less noble elements occurring during dealloying. In fact, it is known that the nitric acid has a high aggressive effects on the dissolution of copper, that constitute about the 30% of the atoms present in the alloy. Therefore, if the surface is rapidly deprived from the less noble elements, an higher diffusivity can be expected for the Au atoms and, therefore, the formation of larger crystals can be justified that lead to the formation of larger ligaments. This observation is suggested by the scattering domain sizes collected by Rietveld analysis of the XRD patterns that show that similar crystals of about 50 nm are present in the samples produced using $HClO_4$ and H_2SO_4 while slightly larger scattering domains are determined for the sample obtained by using HNO_3.

4. Conclusions

The electrochemical behaviour and the dealloying process of $Au_{40}Cu_{28}Ag_7Pd_5Si_{20}$ amorphous ribbon have been studied in 1 M HNO_3, 1 M H_2SO_4 and 1 M $HClO_4$.

For all electrolytes, dealloying is complete after 6 hours and results in the formation of a free

standing nanoporous structure composed entirely of nominal pure Au. Characterization by XRD, Rietveld analysis and SEM images gives a similar size of crystalline domains and dimensions of pores and ligaments for dealloying in sulphuric and perchloric acid while a slightly larger size has been found in nitric acid.

The first stages of dealloying were studied by means of HRTEM observations and an ultrafine nanoporous structure was evidenced, with nanopores and randomly oriented nanocrystals of a few nm size. A low diffusivity (1×10^{-19} m^2s^{-1}) was evaluated and a change in growth mechanism was suggested after the first stages of the process when impingement occurs.

Therefore, different morphologies can be produced starting from a gold based amorphous metal, depending on the time and procedure of dealloying, which can be tailored to exploit different chemical and physical properties. In particular, free standing and flexible nanoporous materials can be obtained for completely dealloyed gold based glassy ribbons using long processing times. In this case, ligaments are of the order of 100 nm or higher according to the electrolyte used for the process. If a short time of dealloying is used, a fine nanoporous gold structure with randomly oriented crystals and nanopores can be produced, due to a low diffusivity acting during the initial stages of the process. The latter material is expected to have enhanced chemical and physical properties with respect to porous metals with coarsened morphology.

Acknowledgements

Work performed for MIUR-Progetto di Rilevante Interesse Nazionale 2008. Fondazione S. Paolo is acknowledged for support to CdE NIS.

References

[1] X.Y. Lang, H. Guo, L.Y. Chen, A. Kudo, J.S. Yu, W. Zhang, A. Inoue, M.W. Chen, Novel nanoporous Au-Pd Alloy with high catalytic activity and excellent electrochemical stability, Journal of Physical Chemistry C, 114 (2010) 2600-2603

[2] A. Schaefer, D. Ragazzon, A. Wittstock, L. E. Walle, A. Borg, M. Baumer, A. Sandel, Toward controlled modification of nanoporous gold. A detailed surface science study on cleaning and oxidation, Journal of Physical Chemistry C (2012), 116, 4564−4571

[3] H.Min, N.Sullivan, D.Allara, S.Tadigadapa, Nanoporous gold: A high sensitivity and specificity biosensing substrate, Procedia Engineering 25 (2011) 1469 – 1472

[4] G. Li, X. Song, Z. Sun, S. Yang, B. Ding, S. Yang, Z. Yang, F. Wang, Nanoporous Ag prepared from the melt-spun Cu-Ag alloys, Solid State Sciences, 13 (2011) 1379-1384

[5] H.-J. Jin, J. Weissmüller, Bulk nanoporous metal for actuation, Advanced Engineering Materials, 12 (2010) 714-723.

[6] J.Erlebacher, Mechanism of coarsening and bubble formation in high-genus nanoporous metals, Physical Review Letters 106 (2011) 225504

[7] J. Erlebacher, R. Seshadri, Hard materials with tunable porosity, MRS Bulletin, 34 (2009) 561-568

[8] S.V. Petegem, S. Brandstetter, R. Maass, A.M. Hodge, B.S. El-Dasher, J.r. Biener, B. Schmitt, C. Borca, H.V. Swygenhoven, On the microstructure of nanoporous gold: An X-ray diffraction study, Nano Letters, 9 (2009) 1158-1163

[9] H.W. Pickering, P.J. Byrne, On Preferential Anodic Dissolution of Alloys in the Low Current Region and the Nature of the Critical Potential, Journal of The Electrochemical Society, 118 (1971) 209-215

[10] H.W. Pickering, Characteristic features of alloy polarization curves, Corrosion Science, 23 (1983) 1107-1120.

[11] K. Sieradzki, N. Dimitrov, D. Movrin, C. McCall, N. Vasiljevic, J. Erlebacher, The dealloying critical potential, Journal of The Electrochemical Society, 149 (2002) B370-B377

[12] D.M. Artymowicz, J. Erlebacher, R.C. Newman, Relationship between the parting limit for de-alloying and a particular geometric high-density site percolation threshold, Philosophical Magazine, 89 (2009) 1663-1693

[13] F. Scaglione, P. Rizzi, L. Battezzati, De-alloying kinetics of an Au-based amorphous alloys, Journal of Alloys and Compounds, 536 (SUPPL.1), S60-S64

[14] G.S. Duffó, S.B. Farina, J.R. Galvele, Stress corrosion cracking of 18 carat gold, Corrosion Science, 46 (2004) 1-4

[15] J.D. Fritz, B.W. Parks, H.W. Pickering, Coherency stress and transgranular stress corrosion cracking of Cu-18Au alloy, Scripta Metallurgica, 22 (1988) 1063-1068

[16] K. Sieradzki, R.C. Newman, Stress-corrosion cracking, Journal of Physics and Chemistry of

Solids, 48 (1987) 1101-1113

[17] S.M. L. Lutterotti, H.-R. Wenk,, MAUD (Material Analysis Using Diffraction) is released under free license of the authors. Available at: http://www.ing.unitn.it/wmaud/index.html.

[18] Z. Zhang, Y. Wang, Y. Wang, X. Wang, Z. Qi, H. Ji, C. Zhao, Formation of ultrafine nanoporous gold related to surface diffusion of gold adatoms during dealloying of Al 2Au in an alkaline solution, Scripta Materialia, 62 (2010) 137-140

[19] L.H. Qian, M.W. Chen, Ultrafine nanoporous gold by low-temperature dealloying and kinetics of nanopore formation, Applied Physics Letters, 91 (2007) 083105

[20] G. Andreasen, M. Nazzarro, J. Ramirez, R.C. Salvarezza, A.J. Arvia, Kinetics of particle coarsening at gold electrode/electrolyte solution interfaces followed by in situ scanning tunneling microscopy, Journal of The Electrochemical Society, 143 (1996) 466-471

[21] A. Dursun, D.V. Pugh, S.G. Corcoran, Dealloying of Ag-Au alloys in halide-containing electrolytes. Affect on critical potential and pore size, Journal of The Electrochemical Society, 150 (2003) B355-B360

[22] J.M. Dona, J. Gonzalez Velasco, Mechanism of surface diffusion of gold adatoms in contact with an electrolytic solution, Journal of Physical Chemistry, 97 (1993) 4714-4719

[23] M.P. García, M.M. Gómez, R.C. Salvarezza, A.J. Arvia, Effect of the solution composition and the applied potential on the kinetics of roughness relaxation at gold electrodes in slightly acid electrolytes, Journal of Electroanalytical Chemistry, 347 (1993) 237-246

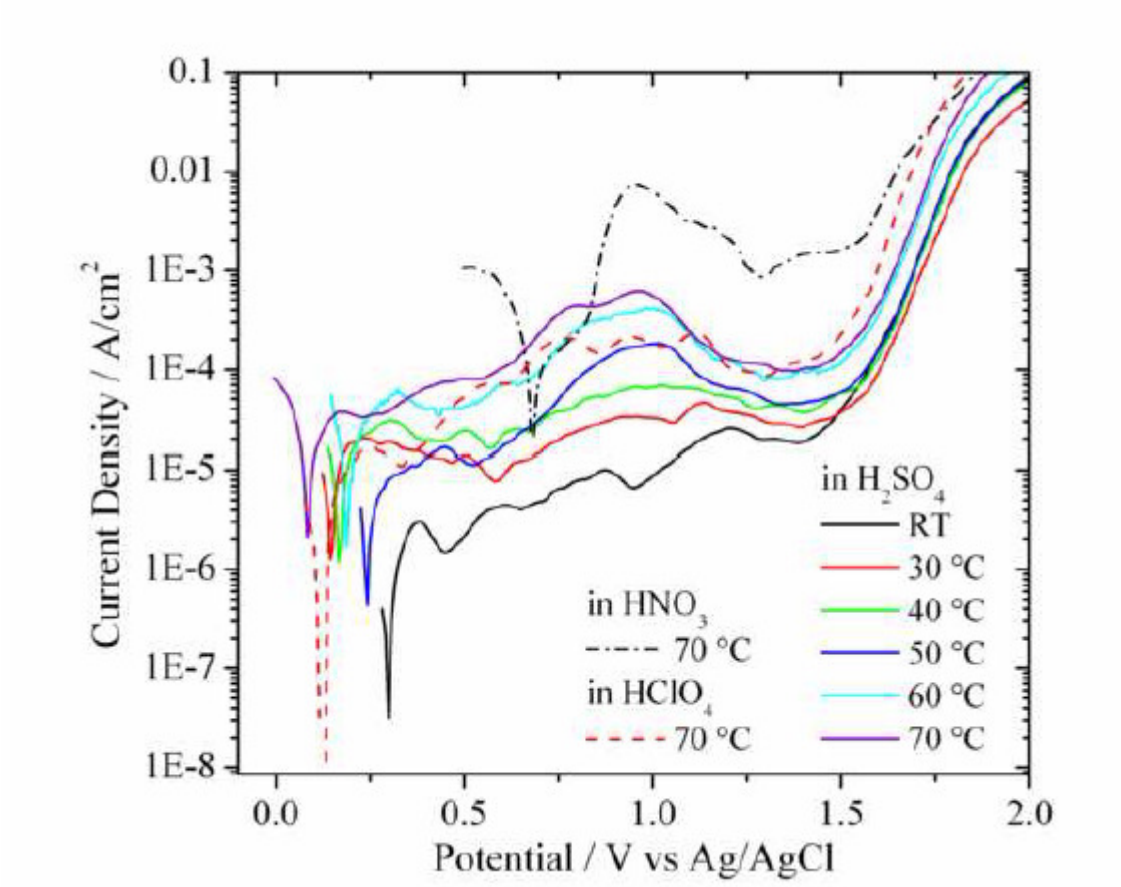

Fig. 1. Polarization curves of the amorphous alloy at various temperatures in 1 M H_2SO_4 and at 70 °C in 1M HNO_3 and 1 M $HClO_4$.

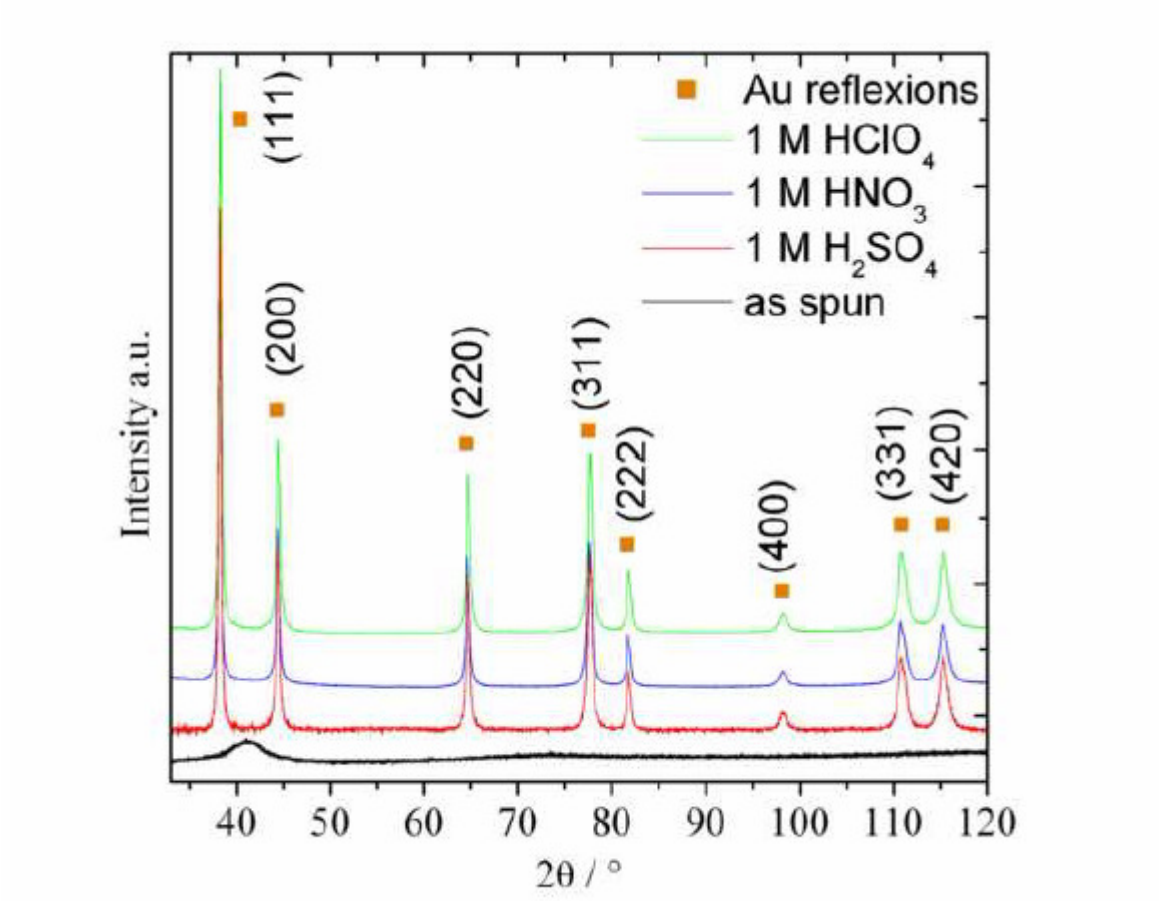

Fig. 2. XRD patterns of the as-spun ribbon and samples after 6 h of dealloying a 70 °C and 1.05V (vs Ag/AgCl) in 1 M H_2SO_4, 1 M $HClO_4$ and 1 M HNO_3.

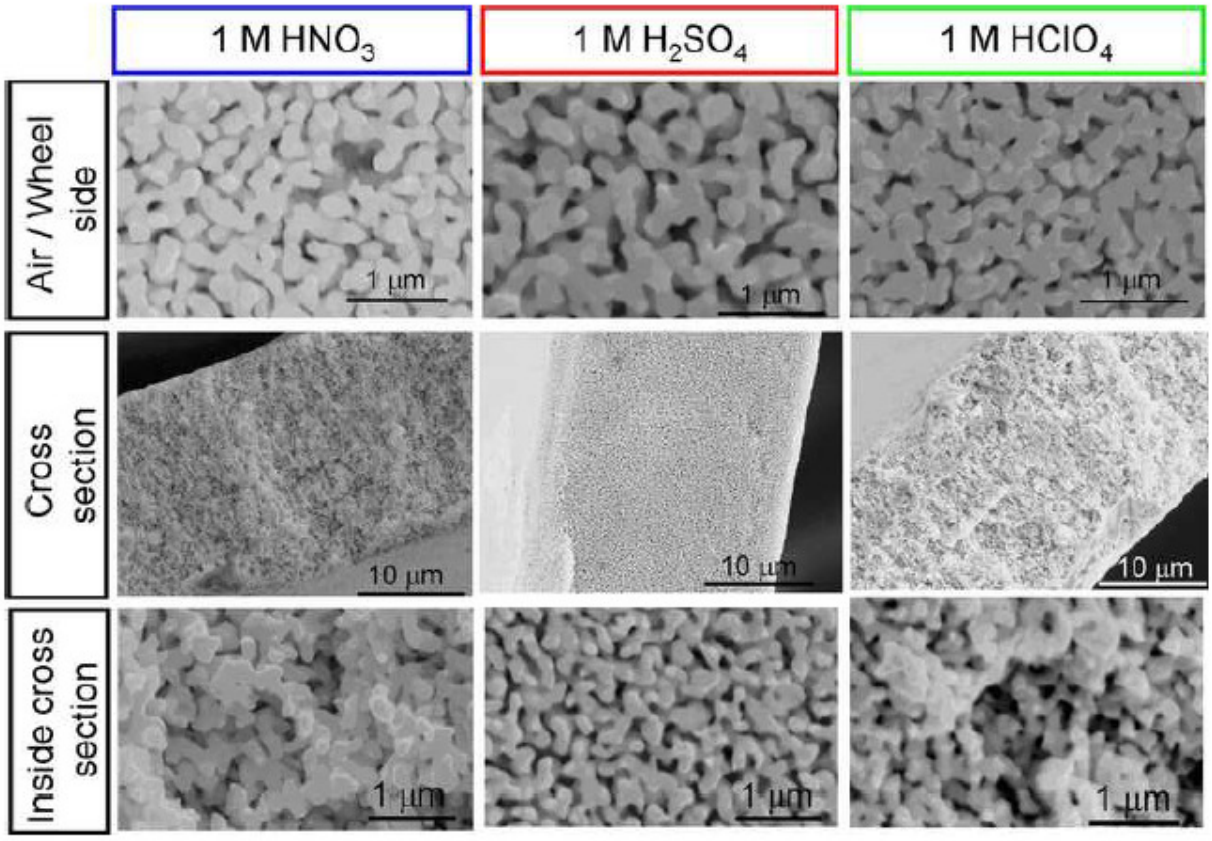

Fig. 3. Secondary electrons SEM images of samples dealloyed in 1 M H_2SO_4, 1 M $HClO_4$ and 1 M HNO_3. Details of ligaments and pores on the air/wheel side and on the cross section.

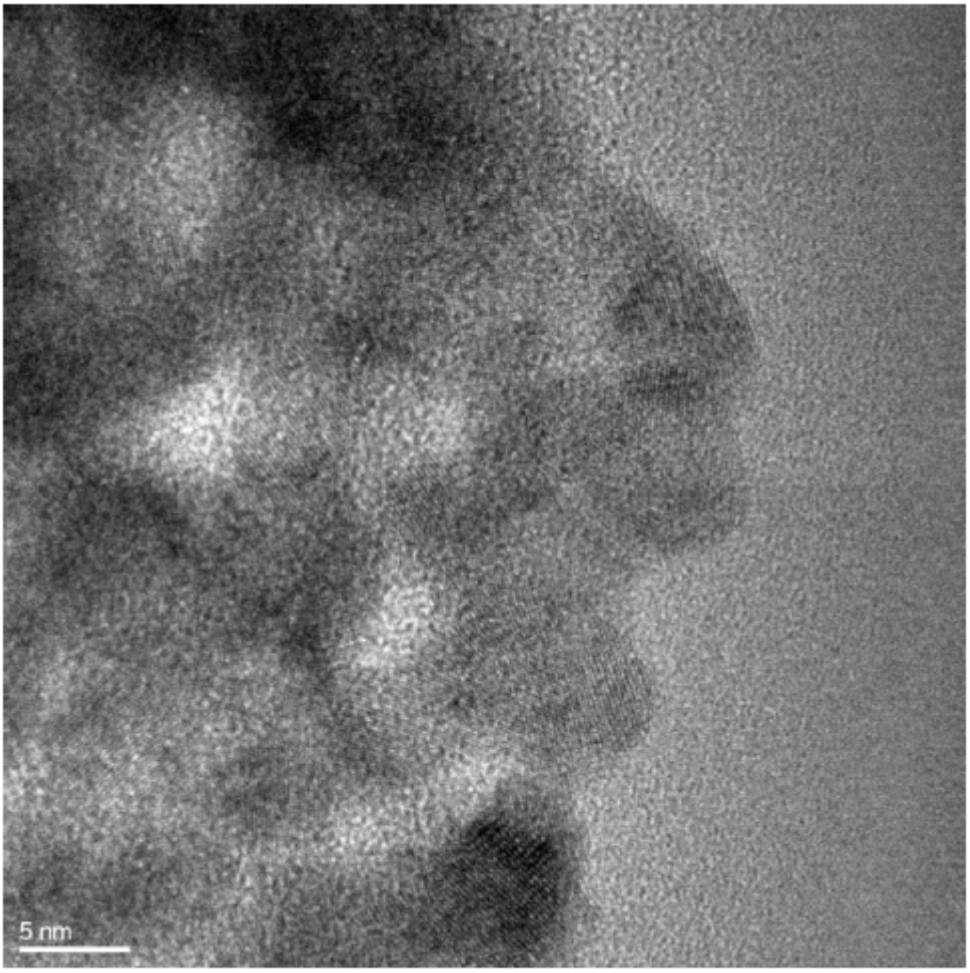

Fig 4. HRTEM image of a sample dealloyed for 30 s in 1 M HNO_3